JOURNAL OF THERMOPHYSICS AND HEAT TRANSFER
Vol. 23, No. 4, October–December 2009

Melting of Steel Spherical Particle in Its Own Liquid: Application to Cladding

Amitesh Kumar* and Subhransu Roy†
Indian Institute of Technology, Kharagpur 721302, India

DOI: 10.2514/1.43112

Blown-powder laser cladding finds its application in manufacturing industries to improve the surface properties of metallic mechanical parts. In the blown-powder laser-cladding process the powder particles go into the superheated melt pool formed by melting of the powder and become the integral part of the substrate coating upon solidification as the laser beam moves away. In the present study, two-dimensional axisymmetric Navier–Stokes and energy equations are solved using the finite volume method to predict the time required for a steel sphere to melt in a melt pool of the same material. The effect of forced convection, characterized by a Reynolds number, and superheat of the melt pool, characterized by a Stefan number, have been studied in detail for a Prandtl number of 0.13. The effect of buoyancy is neglected for the present investigation. It is found that the effect of forced convection on melting time reduction is more pronounced for the low Stefan number case. The rate of melting of the sphere with time under different conditions is also presented. Finally, the heat transfer characteristic is presented by the correlation of a Nusselt number with a Reynolds number and a Stefan number for a Prandtl number of 0.13. The decrease in size of the particle and its change in shape have been presented along with the evolving velocity and temperature field around the particle.

Nomenclature

A	=	porosity function, kg/m^2 s
f_l	=	liquid fraction
Gr	=	Grashof number
h	=	specific sensible enthalpy, J/kg
h_c	=	heat transfer coefficient, W/m^2 °C
k	=	thermal conductivity, W/m^2 °C
Nu	=	Nusselt number
Pr	=	Prandtl number
p	=	pressure, N/m^2
R	=	radius of solid sphere, m
Re	=	Reynolds number
r, z	=	cylindrical coordinate system, m
Ste	=	Stefan number
t	=	time, s
U_∞	=	freestream velocity along z direction, m/s
$\mathbf{V}$	=	velocity vector, m/s
v_r, v_z	=	velocity component in r, z directions, m/s
α	=	thermal diffusivity, m^2/s
Δh_{sl}	=	specific latest heat of fusion, J/kg
ν	=	kinematic viscosity, m^2/s
ρ	=	density, kg/m^3
τ	=	dimensionless time
ψ	=	stream function, kg/s

Subscripts

D	=	diameter
l	=	liquidus
s	=	solidus
0	=	initial condition, that is, at $t = 0$
∞	=	freestream condition

Superscript

$\star$	=	dimensionless variable

Received 9 January 2009; revision received 29 May 2009; accepted for publication 29 May 2009.

*Research Scholar, Department of Mechanical Engineering.
†Professor, Department of Mechanical Engineering; suroy@iitkgp.ac.in (Corresponding Author).

I. Introduction

LASER cladding is one of the techniques which improves the surface properties of metallic mechanical parts, such as the resistance against wear and corrosion. Laser cladding with powder feed has established itself in practice. Some of the applications include the enhancement of the corrosion resistance of the gas turbine blades and improvement of the wear resistance of diesel engine exhaust valves. In the blown-powder laser-cladding process powder particles of diameter 20 to 200 μm are injected into the superheated melt pool with velocity in the range of 0.1–10 m/s. The powder particles melt and mix with the surrounding molten material formed by melting of the powder. Knowledge of the convective heat transfer from a melting metal sphere under such conditions is important for understanding this transport process.

Melting of a solid particle in a superheated fluid of the same or different material has been studied extensively. Kreith et al. [1] performed an experimental and theoretical investigation of rotating metallic spheres in liquid mercury and suggested a correlation for forced convection. Hsu [2] has given an expression for the theoretical Nusselt number for the cases of heat transfer to liquid metals flowing past a single sphere, and flowing past an elliptical rod considering potential flow around the solid object. Anselmo et al. [3] have presented the theoretical and experimental results on the melting of both fully and partially immersed silicon spheres. Numerical and experimental investigations on the melting time of a solid sphere immersed in liquid aluminum and steel have been carried out by Argyropoulos and Mikrovas [4] and Argyropoulos et al. [5]. They have given correlations for forced and natural convection based on the measurement of the melting times of the spheres. More recently, Melissari and Argyropoulos [6,7] have conducted an extensive numerical and experimental analysis of the melting of pure aluminum and AZ91 magnesium alloy in the liquid bath of the same material. In another paper Melissari and Argyropoulos [8] found the correlation for forced convection correlating the Nusselt number to the Reynolds number and the Prandtl number.

There are a few studies on the melting dynamics of nonmetallic spheres at different convective regimes. Kranse and Schenk [9] performed experiments on the free convection melting of a submerged benzene sphere in an excess amount of its own liquid. The

results provided an equation for the Nusselt number in terms of the Grashof number and the Prandtl number. Schenk and Schenkels [10] have considered melting of an ice sphere in the free convection regime. They accounted for the effect of convection inversion due to the anomalous behavior of the thermal expansion coefficient of the water near the temperature of 4°C. The qualitative and quantitative analysis of the convective melting process of ice spheres has been performed by Hao and Tao [11,12]. Mcleod et al. [13] visualized melting of a wax sphere in hot water and calculated the melting rate using a simple theoretical analysis which estimates the melt layer thickness and the heat flux from the fluid.

The importance of buoyancy while studying melting of particles in a superheated liquid has been reported in a few articles. Kreith and his associates [1,14] have studied the effect of mixed convection on the melting of a sphere in a superheated fluid. They suggested that if the buoyancy parameter Gr_D/Re_D^2 based on the diameter of the sphere is less than 0.3, then the natural convection effect is negligible. This value agrees with the theoretical derivation by Sparrow et al. [15]. A numerical study has been conducted by Melissari and Argyropoulos [16] to understand the effect of mixed convection on the total melting time of a particle and they concluded that if the buoyancy parameter Gr_D/Re_D^2 is lower than the range 0.5–1.0, then the total melting time is not affected by the natural convection effects.

The purpose of the present investigation is to develop a mathematical model to analyze the influence of the inflow velocity, characterized by the Reynolds number, and the surrounding fluid temperature typically occurring during cladding, characterized by the Stefan number, on the melting of an immersed solid sphere of steel in a liquid of the same material. Further, a heat transfer correlation has been developed relating the Nusselt number with the Reynolds number and the Stefan number. The role of the Stefan number is important, because it affects the flow characteristic significantly, and very little information is available in the literature in this regard.

II. Mathematical Model

The physical model considered for the present study is that of a solid sphere of steel having initial radius R_0 which is kept at a temperature very close to the solidus temperature. The solid sphere is exposed to a superheated melt with inflow velocity U_∞. During melting of the solid particle the solid–liquid interface will shrink. The surrounding fluid is the molten phase of the solid material. Emphasis is placed on the analysis of constrained melting, which means that both the solid and the liquid have the same density. The schematic diagram in a two-dimensional axisymmetric domain showing the solid particle surrounded by the flowing superheated fluid is presented in Fig. 1.

A. Governing Equations

The flow around the melting sphere is considered to be laminar. Axisymmetric flow of Newtonian and incompressible fluid is considered. As the radius of the particles varies between 10 and 100 μm, the Grashof number is very small and therefore the buoyancy effect is negligible.

The governing equations were nondimensionalized using the initial radius of the solid particle R_0 as the length scale and the heat diffusion speed α/R_0 as the velocity scale. The decision to choose α/R_0 as the velocity scale instead of the freestream velocity was made because the results for melting under zero freestream velocity are also presented. With these length and velocity scales, the nondimensional parameters are

$$r^\star = \frac{r}{R_0} \qquad z^\star = \frac{z}{R_0} \qquad v_r^\star = \frac{v_r}{\alpha/R_0} \qquad v_z^\star = \frac{v_z}{\alpha/R_0}$$

$$\tau = \frac{\alpha t}{R_0^2} \qquad Re = \frac{U_\infty R_0}{\nu} \qquad p^\star = \frac{p}{\rho\alpha^2/R_0^2} \qquad h^\star = \frac{h - h_s}{h_\infty - h_s}$$

$$Ste = \frac{h_\infty - h_s}{\Delta h_{\mathrm{sl}}} \qquad Pr = \frac{\nu}{\alpha}$$

A two-dimensional axisymmetric version of Navier–Stokes equations along with energy transport equation in dimensionless form is presented:

$$\nabla^\star \cdot \mathbf{v}^\star = 0 \tag{1}$$

$$\frac{\partial v_r^\star}{\partial \tau} + (\mathbf{v}^\star \cdot \nabla^\star) v_r^\star = -\frac{\partial p^\star}{\partial r^\star} + Pr\left(\nabla^{\star 2} v_r^\star - \frac{v_r^\star}{r^{\star 2}}\right) + A^\star v_r^\star \tag{2}$$

$$\frac{\partial v_z^\star}{\partial \tau} + (\mathbf{v}^\star \cdot \nabla^\star) v_z^\star = -\frac{\partial p^\star}{\partial z^\star} + Pr\nabla^{\star 2} v_z^\star + A^\star v_z^\star \tag{3}$$

$$\frac{\partial h^\star}{\partial \tau} + (\mathbf{v}^\star \cdot \nabla^\star) h^\star = \nabla^{\star 2} h^\star - \frac{1}{Ste}\left(\frac{\partial f_l}{\partial \tau} + (\mathbf{v}^\star \cdot \nabla^\star) f_l\right) \tag{4}$$

The nondimensional boundary conditions are as follows:

Upstream:

$$0 \le r^\star \le \infty, \quad z^\star = -\infty\text{: } v_r^\star = 0, \quad v_z^\star = RePr, \quad h^\star = 1$$

Downstream:

$$0 \le r^\star \le \infty, \quad z^\star = \infty\text{: } \frac{\partial v_r^\star}{\partial z^\star} = 0, \quad \frac{\partial v_z^\star}{\partial z^\star} = 0, \quad \frac{\partial h^\star}{\partial z^\star} = 0$$

Axis:

$$r^\star = 0, \quad -\infty \le z^\star \le \infty\text{: } v_r^\star = 0, \quad \frac{\partial v_z^\star}{\partial r^\star} = 0, \quad \frac{\partial h^\star}{\partial r^\star} = 0$$

Lateral freestream:

$$r^\star = \infty, \quad -\infty \le z^\star \le \infty\text{: } v_r^\star = 0, \quad v_z^\star = RePr, \quad h^\star = 1$$

The nondimensional initial conditions are as follows:

Solid sphere:

$$t = 0\text{: } h^\star = 0, \quad v_r^\star = v_z^\star = 0$$

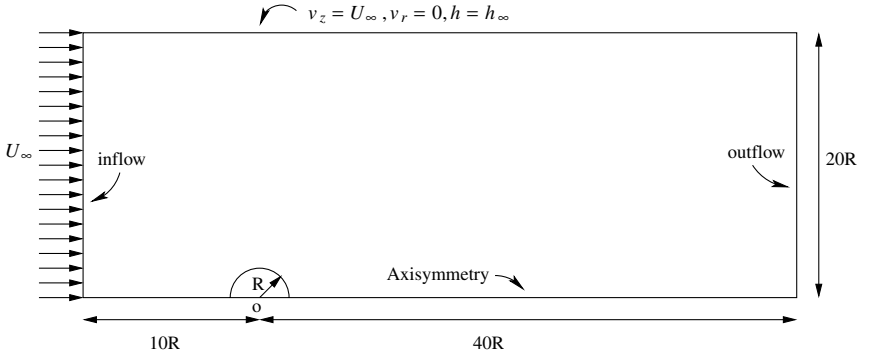

Fig. 1 Schematic diagram of melting of a sphere under forced convection.

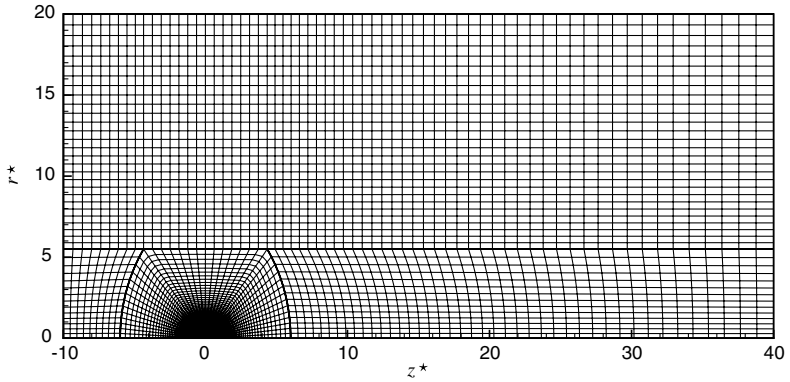

Fig. 2 Computational grid used for the present problem.

Surrounding fluid:

$$t = 0\text{: } h^\star = 1, \quad v_r^\star = v_z^\star = 0$$

It is to be noted that the freestream velocity boundary condition $v_z^\star = RePr$ is implemented through the use of a Reynolds number. To solve the energy equation, a single region (or continuum) enthalpy formulation is implemented. A Darcy law-type porous medium formulation, due to Voller and Prakash [17], is utilized to account for the effect of phase change on the momentum equation. The last term in the momentum Eqs. (2) and (3) is the Darcy damping term $A^\star$ which smoothly connects the solid region (having zero velocity and infinite viscosity) to the liquid metal (having vigorous convection and finite viscosity) through the mushy region. This porosity function is defined as [18]

$$A^\star = \frac{-C_0^\star (1 - f_l)^2}{f_l^3}, \qquad C_0^\star = \frac{C_0 R_0^2}{\rho_0 \alpha_0} \tag{5}$$

where $C_0 = 1.016 \times 10^6$ kg/s m^3. The liquid fraction f_l in the mushy region is calculated using a linear model which is given as follows:

Pure solid:

$$h^\star \le 0\text{: } f_l = 0.0$$

Mushy region:

$$0 \le h^\star \le h_l^\star\text{: } f_l = \frac{h^\star}{h_l^\star}$$

Pure liquid:

$$h^\star \ge h_l^\star\text{: } f_l = 1.0$$

During melting the effective radius $R^\star(\tau)$ of the solid was calculated based on the instantaneous volume $\Omega^\star(\tau)$ of the solid as

$$R^\star(\tau) = \left(\frac{3\Omega^\star(\tau)}{4\pi}\right)^{1/3}, \quad \text{where } \Omega^\star(\tau) = \int_\Omega (1 - f_l) \mathrm{d}\Omega^\star$$

The dimensionless effective radius $R^\star$ is used to capture the decreasing size of the particle during melting. A Nusselt number for the melting solid based on initial radius R_0 is derived in the Appendix. It can be expressed in terms of the nondimensional melting time $\Delta\tau_{\text{melt}}$ of the solid and the Stefan number as shown here,

$$Nu = \frac{2}{3Ste\Delta\tau_{\text{melt}}} \tag{6}$$

B. Solution Approach

The two-dimensional axisymmetric Navier–Stokes equations along with the energy equation were discretized using a structured collocated, nonorthogonal multiblock grid system. Detailed discussion about the structured multiblock system adopted here can be found in Ferziger and Peric [19]. The convective term in the governing equations is discretized using the deferred correction approach which gives second-order accuracy. The diffusive term and the unsteady term are discretized using a central difference scheme and an implicit three time level method (a quadratic backward approximation), respectively, giving second-order accuracy in space and time. The discretized governing equations were solved using the

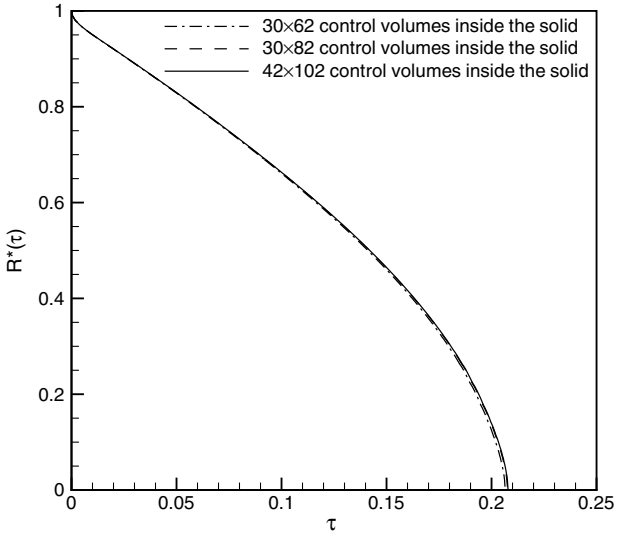

Fig. 3 Variation of nondimensional effective radius with time for $Pr = 0.13$, $Ste = 0.5$, and $Re = 1000$.

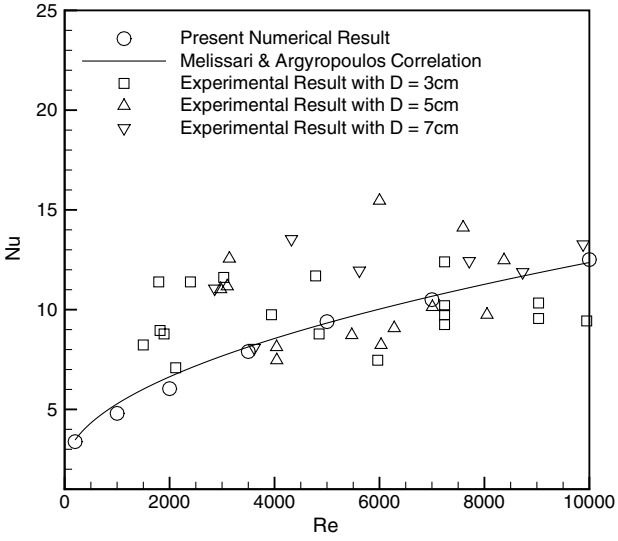

Fig. 4 Nusselt number results for the melting of an aluminum sphere in a 60°C superheated molten aluminum.

Table 1 Thermophysical properties of materials used, SI units [21,22]

Material	ρ_l	μ_l	c_l	α_l	k_l	$h_l - h_{25}$	$h_s - h_{25}$	Δh_{sl}
Iron	7.03×10^3	5.6×10^{-3}	824	6.2×10^{-6}	36	1050×10^3	1050×10^3	247×10^3
SS316	6.88×10^3	8.0×10^{-3}	830	5.0×10^{-6}	28.5	868×10^3	821×10^3	260×10^3

Table 2 Nondimensional total time of melting for two-dimensional and three-dimensional solutions

	$\Delta\tau_{\text{melt}}$		
Ste	3-D solution ($\Delta\tau^{3\text{-D}}_{\text{melt}}$)	2-D solution ($\Delta\tau^{2\text{-D}}_{\text{melt}}$)	% difference $= (\frac{\Delta\tau^{3\text{-D}}_{\text{melt}} - \Delta\tau^{2\text{-D}}_{\text{melt}}}{\Delta\tau^{3\text{-D}}_{\text{melt}}}) \times 100$
0.025	3.347	2.946	11.98
0.25	0.366	0.357	2.46
2.0	0.089	0.089	0.00

semi-implicit method for pressure linked equations (SIMPLE) algorithm [20]. The computational domain size required for an accurate solution depends not only on the size of the sphere but also on the hydrodynamic and thermal conditions to which the sphere is exposed. As we are also solving the case of pure conduction the computational domain boundaries are placed 10 radii upstream, 40 radii downstream, and 20 radii cross stream from the center of the solid particle. A multiblock nonorthogonal grid system having five blocks of 42×102, 42×45, 14×9, 14×42, and 65×28 presented in Fig. 2 was found to be sufficient to resolve the details of flow, temperature fields, and the liquid–solid interface positions based on the comparison of the streamline contours, isoenthalpy contours, and liquid–solid interface positions for various grid densities inside the solid. For example, Fig. 3 shows the variation of nondimensional radius with time for different grid densities inside the solid. The convergence of the result with the increasing number of control volumes can be seen in the plot.

C. Code Validation

The two-dimensional axisymmetric code on the nonorthogonal multiblock grid has been validated against the experimental and numerical results of melting of an aluminum sphere under forced convection in an enclosure by Melissari and Argyropoulos [8]. Although they have considered spheres of different materials, different diameters, and different initial conditions, we have chosen results of immersion of aluminum spheres initially at room temperature in a 60°C superheat bath for comparison. Figure 4 shows the comparison between the numerical prediction by the present method

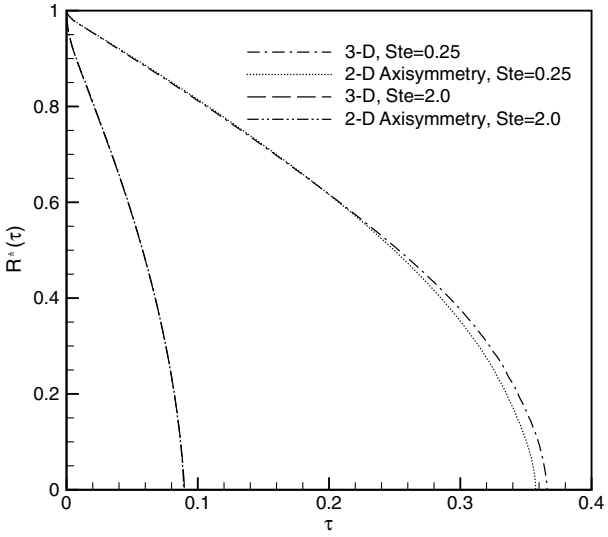

Fig. 5 Variation of nondimensional effective radius with nondimensional time for $Re = 1000$ and $Pr = 0.13$.

Table 3 Nondimensional total time of melting for diffusion-controlled melting, that is, $Re = 0$

Ste	0.025	0.05	0.1	0.25	0.5
$\Delta\tau_{\text{melt}}$	17.954	8.700	4.211	1.640	0.834
Ste	1.0	1.5	2.0	3.0	4.0
$\Delta\tau_{\text{melt}}$	0.452	0.328	0.267	0.205	0.174

and the experimental result by Melissari and Argyropoulos [8]. It is to be noted here that these results are presented for a Nusselt number and a Reynolds number based on the initial diameter D of the sphere denoted by Nu_D and Re_D, respectively. The experimental results are scattered but the matching of the present computed results with the computed results of Melissari and Argyropoulos for this large range of Re_D and small value of *Ste* is good.

III. Results and Discussion

The mathematical model was used to study melting of a solid metal sphere of radius 10 to 100 μm under diffusion control with static surrounding fluid (i.e., $Re = 0$) and melting under forced convection due to relative flow velocity of 0.1 to 10 m/s in the surrounding fluid. The thermophysical properties of SS316 (iron with additional alloying elements) and pure iron at the melting temperature shown in Table 1 are used as reference properties to evaluate different scales and range of dimensionless parameters. Depending on the amount of elements added to iron, its thermophysical properties vary a little; however, the Prandtl number of 0.13 which is equal to that of iron has been used. Such a low value of Prandtl number is typical of many metals. It was found that the thermophysical properties of common metals beyond the melting point are very scarce, and if available, it may go only up to 200 to 300°C beyond the melting point [21,22]. In this temperature range the thermal conductivity of common metals can vary by as much as 5%. Results of calculations are presented here where the temperature of the molten metal surrounding the solid goes close to the evaporation temperature. The melting time and the rate of melting which is related to the temperature and flow conditions of the surrounding fluid were studied. The streamline pattern and the specific sensible enthalpy field during melting with convection are also presented.

For flow past an isothermal sphere the axisymmetry is broken for $Re_D > 200$ [23–25]. For melting of a sphere due to forced convection, there also exist conditions under which axisymmetry is broken. A few three-dimensional solutions were performed for forced convection melting of a sphere to ascertain whether the present range of parameters for which two-dimensional computations were obtained remain axisymmetric even when three-dimensional computations are performed. We have solved the three-dimensional Navier–Stokes equations along with the energy equation for a few cases and realized that for most of the cases studied in this paper the two-dimensional axisymmetric solutions provide not only enthalpy and flowfields similar to the three-dimensional solutions but also the total

Table 4 Effect of convection on nondimensional total time of melting

	$\Delta\tau_{melt}$ for $Pr = 0.13$				
Ste	$Re = 1.0 \times 10^2$	$Re = 2.5 \times 10^2$	$Re = 5.0 \times 10^2$	$Re = 7.5 \times 10^2$	$Re = 1.0 \times 10^3$
0.025	8.9461	6.1707	4.3015	3.4584	2.9461
0.05	4.5723	3.1600	2.2092	1.7753	1.5138
0.1	2.3815	1.6546	1.1601	0.9315	0.7931
0.25	1.0592	0.7423	0.5231	0.4200	0.3572
0.5	0.6074	0.4292	0.3034	0.2441	0.2075
1.0	0.3698	0.2646	0.1885	0.1521	0.1298
1.5	0.2846	0.2065	0.1483	0.1212	0.1029
2.0	0.2397	0.1761	0.1277	0.1038	0.0891
3.0	0.1915	0.1439	0.1057	0.0866	0.0745
4.0	0.1723	0.1302	0.0936	0.0774	0.0669

time of melting within 3% of the three-dimensional solutions. Table 2 presents the nondimensional total time of melting for $Re = 1000$ and $Pr = 0.13$ and the Stefan number in the range 0.025–2.0, and Fig. 5 compares the two-dimensional axisymmetric and three-dimensional solutions for the variation of nondimensional effective radius with nondimensional time. It can be noticed that variation of the nondimensional effective radius with the nondimensional time is almost similar for the two-dimensional axisymmetric and the three-dimensional solutions except for very low Stefan numbers. Therefore, we have considered the two-dimensional axisymmetric model for the numerical simulation.

A. Total Time of Melting and Rate of Melting

In diffusion-controlled melting (i.e., fluid at rest) only the energy Eq. (4) has to be solved and the solid particle remains a perfect sphere at all times with the radius decreasing with the passage of time. Table 3 gives the nondimensional total time of melting for the diffusion-controlled melting at $Re = 0$.

To study the effect of convection, numerical simulations were performed for five Reynolds numbers, 10 Stefan numbers (the maximum value of the Stefan number is limited by the boiling point of the liquid metal), and Prandtl number of 0.13. The total time of melting for 50 different sets of Reynolds numbers and Stefan numbers considered in the present study is summarized in Table 4. With the increase in Reynolds number the convective heat transfer increases, which results in faster melting of the solid particle. Also by increasing the Stefan number the temperature difference between the surrounding fluid and the solid particle increases thereby enhancing the melting rate.

The Nusselt number for the sphere having initial radius R_0 is expressed in terms of the total time of melting and the Stefan number as shown in Eq. (6). By performing the least square fitting of the computed values in Tables 3 and 4, a correlation between Nusselt number, Stefan number, and Reynolds number in the range $0.025 \leq Ste \leq 4.0$ and $0 \leq Re \leq 1.0 \times 10^3$ is obtained. The resultant correlation for the Nusselt number as a function of the Reynolds number and the Stefan number is given by Eq. (7) with a standard deviation $\sigma_{corr} = 2.2\%$,

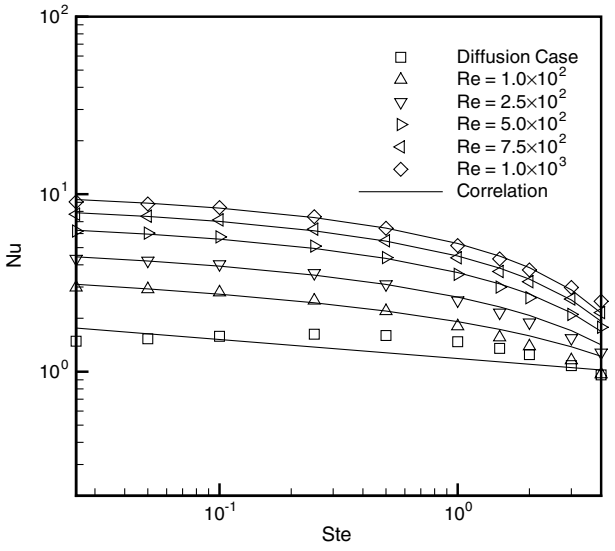

Fig. 6 Dependency of Nusselt number on Stefan number for different Reynolds number at $Pr = 0.13$.

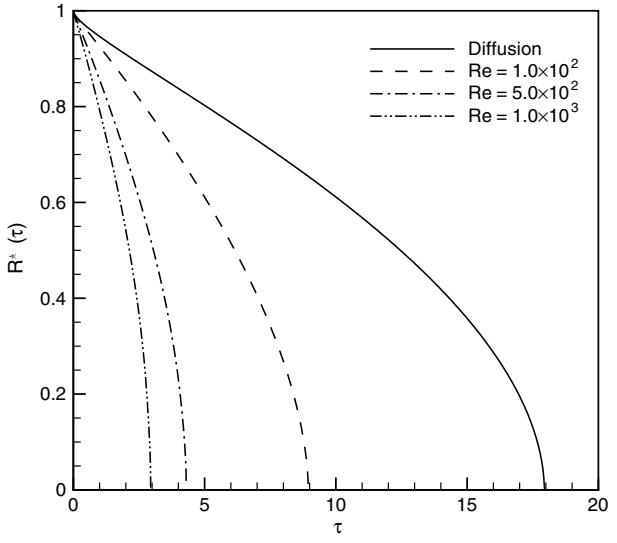

a) Ste = 0.025

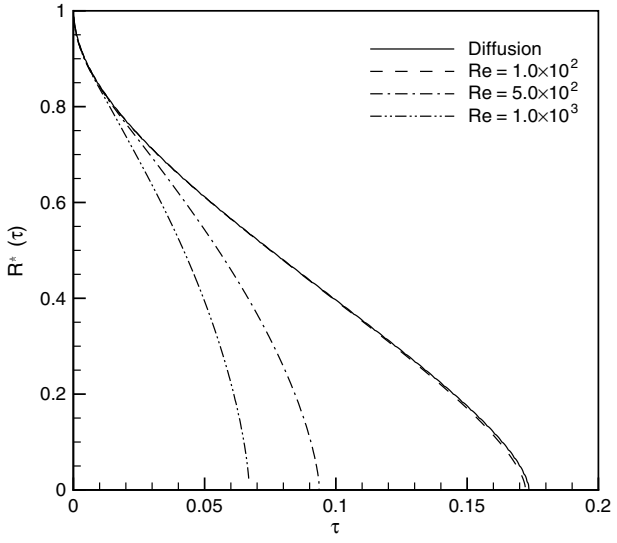

b) Ste = 4.0

Fig. 7 Variation of nondimensional effective radius with nondimensional time for $Pr = 0.13$.

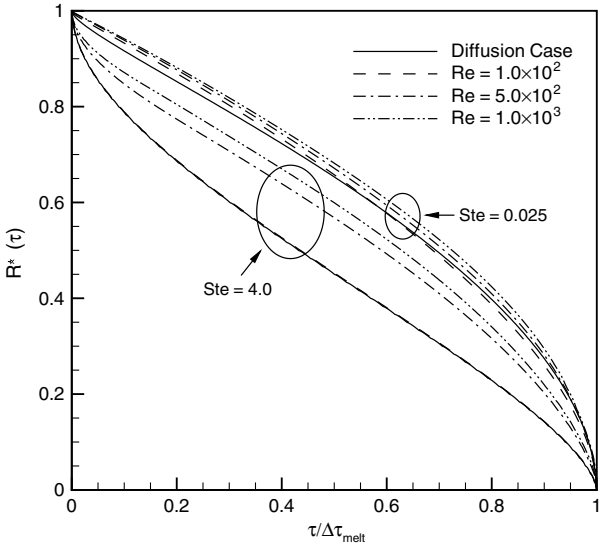

Fig. 8 Variation of nondimensional effective radius with fraction of time for $Pr = 0.13$.

$$Nu = \frac{2}{3Ste\Delta\tau_{\text{melt}}} = (1.187 + (-0.977 + Ste^{-0.013})Re^{3/4}Ste^{1/4})Ste^{-0.107} \quad \text{for } Pr = 0.13 \tag{7}$$

Figure 6 shows the numerical data points for the Nusselt number along with the correlation curve and depicts the dependency of the Nusselt number on the Stefan number for a different Reynolds number. It can be seen from the figure that the Nusselt number increases with an increase in Reynolds number and it decreases with an increase in the Stefan number for the convection case. The pure diffusion case shows a different pattern; the Nusselt number increases slightly up to $Ste = 0.025$, but thereafter it slowly decreases with an increase in Stefan number. For convective cooling the Nusselt number decrease is large for small Stefan numbers and decreases slowly with an increase in the Stefan number. It is of interest to observe that the convection effect is decreasing with an increase in the Stefan number.

During melting with convection the particles do not remain spherical; therefore the effective radius based on volume was calculated during melting. Figure 7 shows the decrease of the

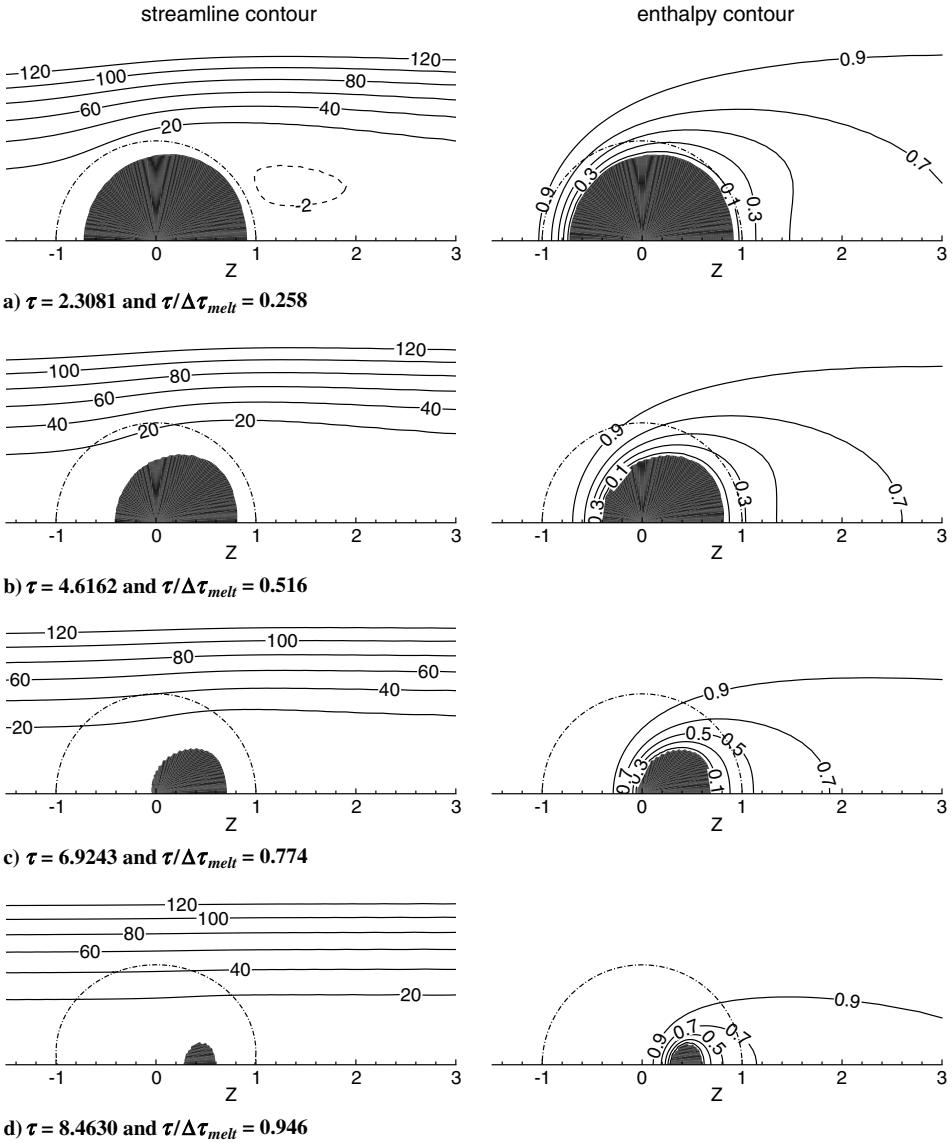

a) $\tau = 2.3081$ and $\tau/\Delta\tau_{melt} = 0.258$

b) $\tau = 4.6162$ and $\tau/\Delta\tau_{melt} = 0.516$

c) $\tau = 6.9243$ and $\tau/\Delta\tau_{melt} = 0.774$

d) $\tau = 8.4630$ and $\tau/\Delta\tau_{melt} = 0.946$

Note: the stream function values are divided by Prandtl number *i.e.,* ψ/Pr.

Fig. 9 Streamlines and isoenthalpy contours for $Re = 1.0 \times 10^2$, $Ste = 0.025$, and $Pr = 0.13$ at four different instants.

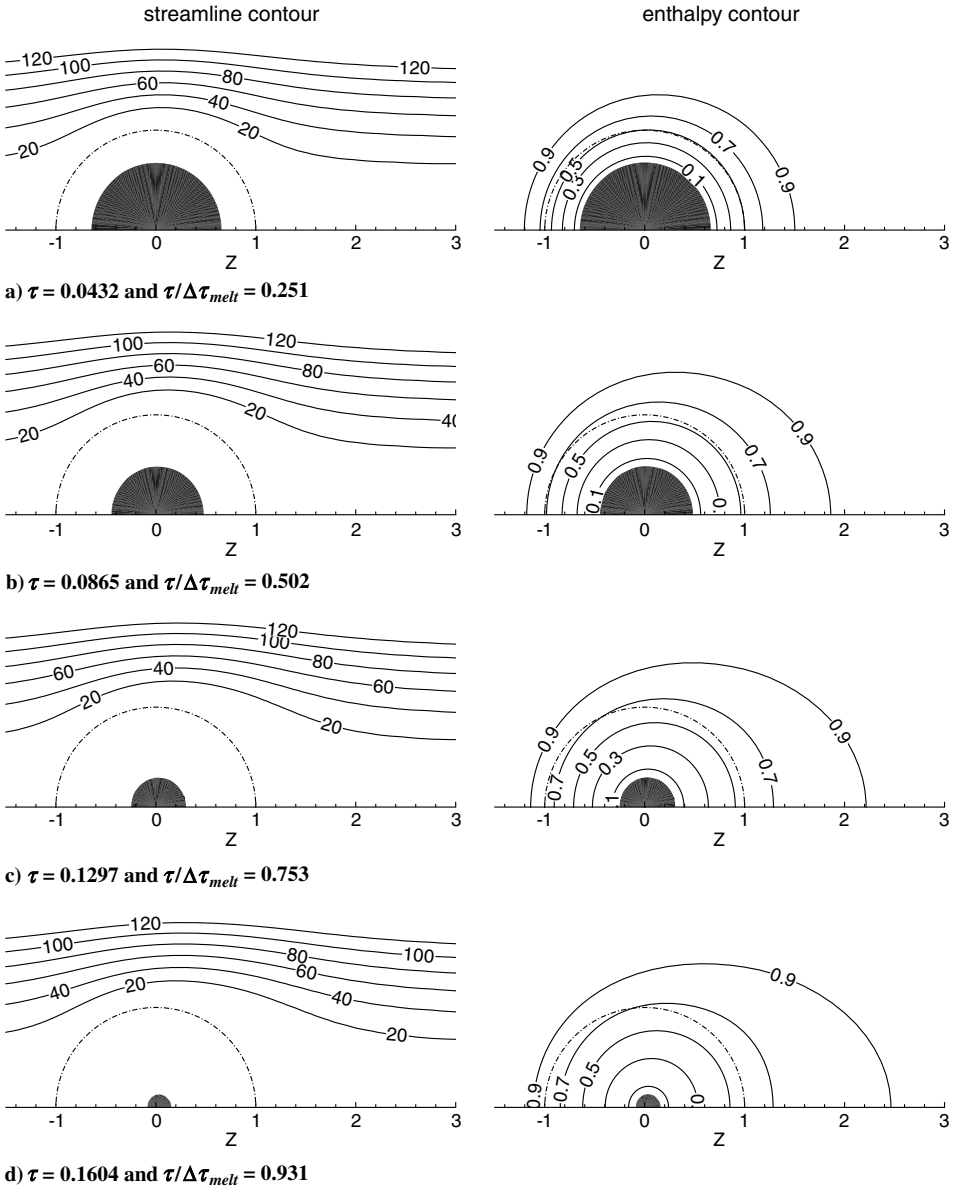

Note: the stream function values are divided by Prandtl number *i.e.,* ψ/Pr.

Fig. 10 Streamlines and isoenthalpy contours for $Re = 1.0 \times 10^2$, $Ste = 4.0$, and $Pr = 0.13$ at four different instants.

dimensionless effective radius with the dimensionless time during melting for the Stefan number of 0.025 and 4.0 for three different Reynolds numbers (100, 500, 1000). A decrease of the total melting time with an increase in Reynolds number is reflected in Fig. 7. The decrease of effective particle radius with time for convection is compared with that of pure conduction shown as a solid line in Fig. 7. As the Reynolds number increases, signifying stronger convective heat transfer, the time required for melting decreases much below the conduction limit. However, it is observed that with higher Stefan number it requires a much stronger convection current for the melting to be faster than that of the pure conduction case.

Figure 8 shows the decrease of dimensionless effective radius with the fraction of melting time during melting for a Stefan number of 0.025 and 4.0 for three different Reynolds numbers (100, 500, 1000). This change in the time scale to fraction of melting time has resulted in the radius variation with time falling within a narrow band close to that of diffusion-controlled melting depicted by a solid line. The melting rate of the sphere becomes faster toward the end as the surface area to solid volume ratio increases with a decrease in radius. For each set of Reynolds numbers, the higher Stefan number value of 4.0 makes the rate of decrease of dimensionless radius with fraction of melting time faster initially. If the Stefan number is decreased to 0.025 the decrease of effective dimensionless radius with fraction of melting time for all the Reynolds numbers becomes very close to that of the diffusion-controlled melting.

B. Streamline and Enthalpy Field During Melting

The flow (streamlines) and enthalpy field around the particle whose shape changes during melting were studied for Reynolds numbers of 100, 250, 500, 750, and 1000 and Stefan numbers of 0.025, 0.05, 0.1, 0.25, 0.5, 1.0, 1.5, 2.0, 3.0, and 4.0, but results have been presented only for the slow flow rate of $Re = 100$ and fast flow rate of $Re = 1000$ for different surrounding fluid conditions of a low superheat value of $Ste = 0.025$ and high superheat value of $Ste = 4.0$ in Figs. 9–12. In each figure the particle shape and the surrounding flow and temperature field have been captured at four instances during the lifetime of the particle before it completely melts. Only one-half of the two-dimensional region on one side of the symmetry axis (angular symmetry) has been shown; the left columns of plots show the streamline contours and the right columns of plots show the enthalpy contours. The original position of the sphere before the start of melting is denoted by dash-dotted semicircles with center (0,0) and dimensionless radius 1, and the shaded areas

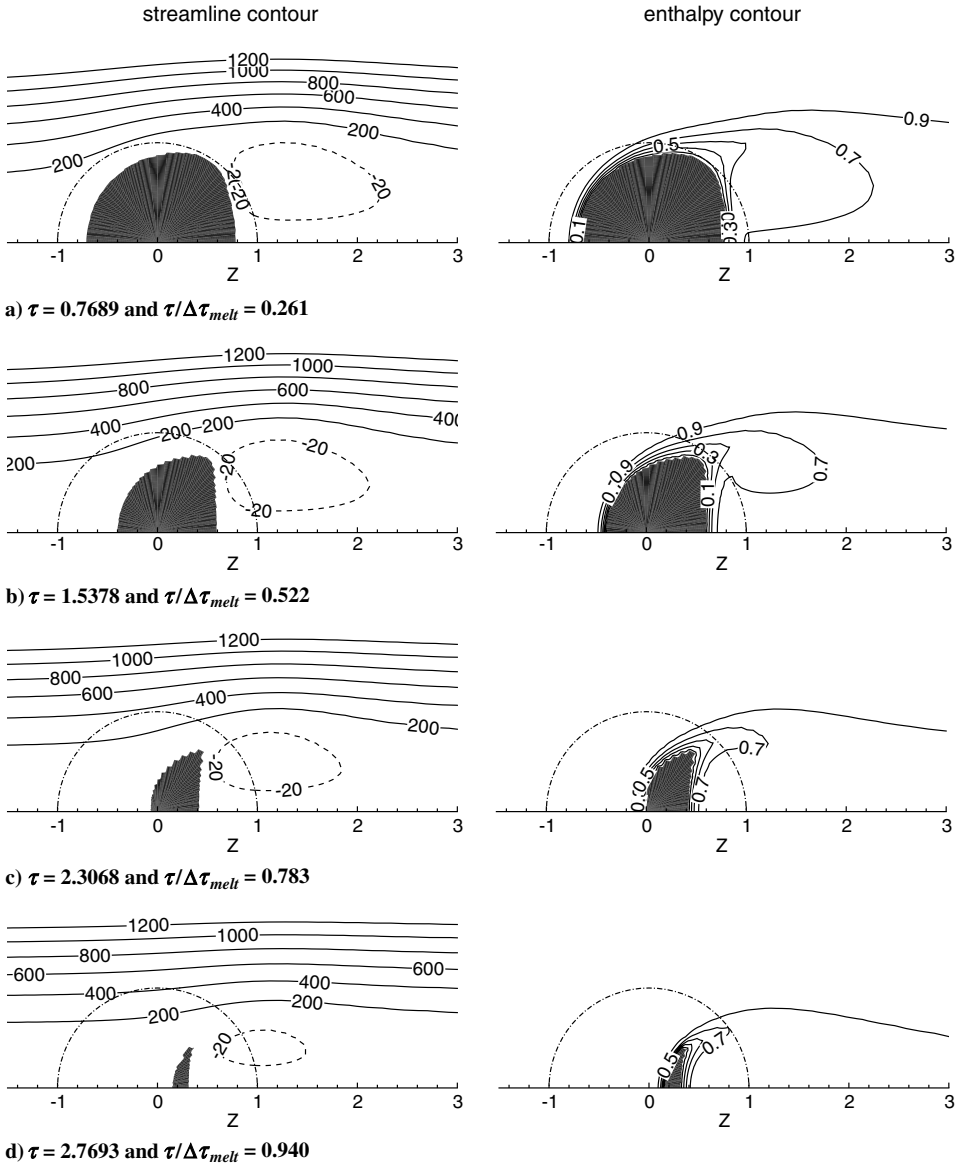

Note: the stream function values are divided by Prandtl number *i.e.,* Ψ/Pr.

Fig. 11 Streamlines and isoenthalpy contours for $Re = 1.0 \times 10^3$, $Ste = 0.025$, and $Pr = 0.13$ at four different instants.

bounded by lines of dimensionless enthalpy contours $h = 0$ indicate the solid phase at a given instant during melting. Comparing the shaded regions to the original particle positions one can find the amount of melting in different directions. The streamline contours show the nature of the flow pattern around the solid particle; the clockwise flow recirculation is denoted by dashed lines.

1. Slow Flow Case, Re = 100

Figure 9 shows the instantaneous contours of streamlines and enthalpy fields for $Re = 100$ and $Ste = 0.025$ at the fraction of melt times $\tau/\Delta\tau_{\text{melt}} = 0.258$, 0.516, 0.774, and 0.946. The two-dimensional (angular symmetry) results indicate that the boundary layer separates in the downstream region and produces a wake represented by clockwise recirculation on one side of the symmetry axis and its mirror image (not shown) will appear on the other side of the symmetry axis. It is observed that the melting is faster in the upstream region and slower in the downstream region where a wake is formed. When the heat transfer is dominated by diffusion the enthalpy contours are concentric with the initial position of the sphere. The presence of convection enhances the melting in the upstream portion of the solid and the enthalpy contours deviate from being concentric rings and are pushed away by the recirculating wake in the downstream region of the solid. The circulatory flowfield in the wake region supports the formation of a cold plume bounded by enthalpy contour $h = 0.7$. As the particle melts the wake and the cold plume shorten and finally vanish. In spite of the different melting rate in the upstream and downstream regions due to convection, the shape of the solid phase remains almost spherical throughout the melting process for this low Reynolds number flow. The flowfield and heat transfer characteristics become closer to a diffusion dominated case with an increase in Stefan number to 4.0 as shown in Fig. 10. Throughout the melting process, the enthalpy contours are closer to concentric rings indicating the dominance of the conduction mode of heat transfer (Fig. 10). No noticeable flow separation took place during the entire melting process. This melting is mainly caused by conduction due to a high Stefan number of 4.0 and the total time of melting decreased to 0.1723 as compared to 8.9461 at the low Stefan number value of $Ste = 0.025$.

2. Fast Flow Case, Re = 1000

Figure 11 shows the instantaneous contours of streamlines and enthalpy fields for $Re = 1000$ and $Ste = 0.025$ at the fraction of melt times $\tau/\Delta\tau_{\text{melt}} = 0.261, 0.522, 0.783$, and 0.940. With an increase in the Reynolds number the effect of convection can be seen from the beginning of the melting process. The enthalpy contours deviate further from being concentric rings even at the beginning of melting

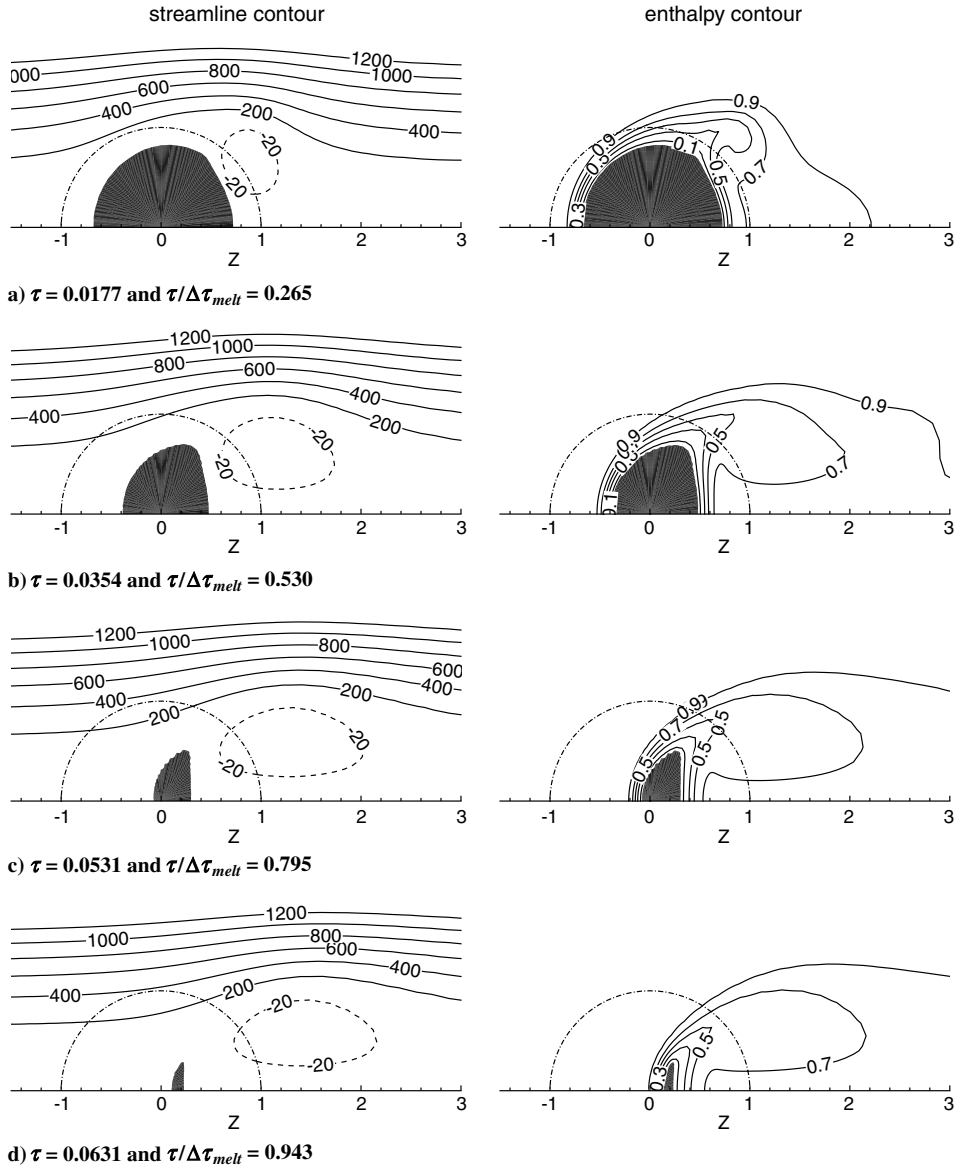

Note: the stream function values are divided by Prandtl number *i.e.,* ψ/Pr.

Fig. 12 Streamlines and isoenthalpy contours for $Re = 1.0 \times 10^3$, $Ste = 4.0$, and $Pr = 0.13$ at four different instants.

and the solid portion is shaped as an oblate spheroid. Even the strength of the clockwise rotating recirculating cell in the wake region increases markedly due to higher Reynolds number and sustains a cold plume with a kidney-shaped cross section during the first half-time of the life of the solid. The two-dimensional (angular symmetry) plots reveal that the downstream rear portion of the solid remains almost flat. It is interesting to note that the melting rate of the front and rear regions is much faster than the sides. The circulation in the wake region enhances the heat transfer from the solid boundary near the axis at the rear position. Therefore, the local melting rate increases causing the rear portion to become flat. In turn, the flow pattern is also affected.

Figure 12 shows the instantaneous contours of streamlines and enthalpy fields for $Re = 1000$ and $Ste = 4.0$ at the fraction of melt times $\tau/\Delta\tau_{\text{melt}} = 0.265, 0.530, 0.795$, and 0.943. With an increase in the Stefan number by 160-fold from 0.025 to 4.0 the dimensionless melting time decreased by 40-fold from 2.9461 to 0.0669 due to high superheat of the surrounding fluid. It can be easily observed from the plots that the clockwise recirculating cell in the wake region grows slowly during the first half of the lifetime of the particle for $Ste = 4.0$ as compared to the corresponding case of $Ste = 0.025$. The wake becomes large in the second half of the lifetime of the particle giving rise to a cold plume with a kidney-shaped cross section in a two-

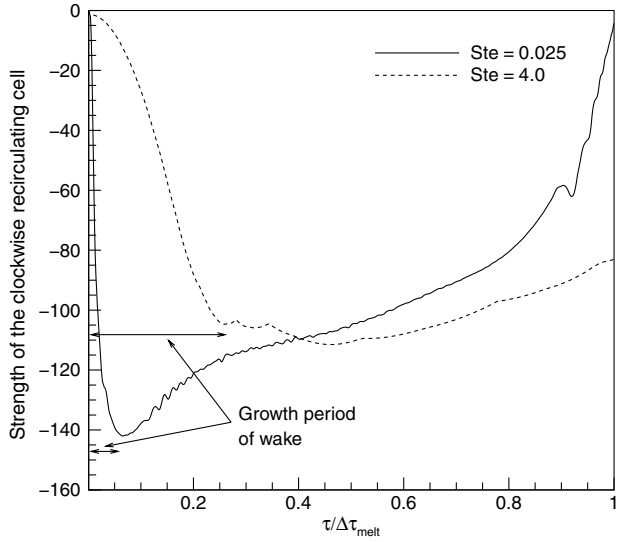

Fig. 13 Variation of the strength of clockwise recirculation with a fraction of melt time for $Re = 1.0 \times 10^3$ and $Pr = 0.13$.

dimensional plane (angular symmetry) and retain its size even at $\tau/\Delta\tau_{\text{melt}} = 0.943$ as opposed to the decreasing size of the wake for a low Stefan number during the same time period. The strength of the recirculating cell is defined as the value of the stream function at the center of the cell. Figure 13 shows the variation of the strength of the clockwise recirculating cell in the wake region with the fraction of melting time; after an initial growth phase, the wake stabilizes for a while and finally vanishes when the melting is complete. However, for the high $Ste = 4.0$ the wake stays strong for a longer time up to the end of melting before it vanishes (not shown in the plot).

IV. Conclusions

In the present numerical investigation, the total dimensionless melting time of a sphere due to forced convection under different values of Reynolds number has been studied extensively for different values of Stefan numbers. It was found that the dimensionless total time of melting $\Delta\tau_{\text{melt}}$ varies inversely with the Stefan number for the diffusion-controlled melting case. The dimensionless total melting time $\Delta\tau_{\text{melt}}$ reduces with an increase in Reynolds number as $Re^{-3/4}$ and it reduces with increases in Stefan number as $Ste^{-5/4}$ approximately for $Pr = 0.13$. The Nusselt number for the sphere at the beginning of melting can be expressed in terms of the dimensionless total time of melting and the Stefan number. A correlation formula is presented between the Nusselt number, the Stefan number, and the Reynolds number for the range $0 \le Re \le 1.0 \times 10^3$, $0.025 \le Ste \le 4.0$, and $Pr = 0.13$. The decrease in the size of the particle and its change in shape has been presented along with the evolving velocity and enthalpy field around the particle. The growth of the recirculation (wake) and the cold plume behind the particle and its gradual decline as the particle melts has been presented.

Appendix: Nusselt Number for a Melting Sphere

The heat transfer coefficient for the melting sphere of radius R is obtained by performing a heat balance over the time interval dt as

$$h_c(h_\infty - h_s) = \rho c \Delta h_{\text{sl}} \frac{\mathrm{d}R}{\mathrm{d}t} \tag{A1}$$

where all the variables are dimensional.

Here $h_c = h_c(R)$ is the instantaneous heat transfer coefficient for the particle. Assuming that the Nusselt number can be expressed as the function of the Reynolds number for a laminar boundary layer [26] we obtain

$$Nu \propto Re^{1/2} \quad \text{and} \quad h_c \propto \frac{1}{\sqrt{R}} \qquad h_c(R) = h_{c0}\sqrt{R_0}\frac{1}{\sqrt{R}} \tag{A2}$$

where h_{c0} is the heat transfer coefficient for the initial sphere of radius R_0 at time $t = 0$. Substituting h_c from Eq. (A2) into Eq. (A1) and integrating from initial radius R_0 to zero over the time interval Δt_{melt} we get the Nusselt number as

$$\frac{\int_{R_0}^{0}\sqrt{R}\mathrm{d}R}{h_{c0}\sqrt{R_0}} = \frac{\alpha(h_\infty - h_s)}{k\Delta h_{\text{sl}}}\int_0^{\Delta t_{\text{melt}}}\mathrm{d}t$$

$$\frac{2R_0}{3h_{c0}} = \frac{\alpha(h_\infty - h_s)}{k\Delta h_{\text{sl}}}\Delta t_{\text{melt}}$$

$$Nu = \frac{h_{c0}R_0}{k} = \frac{2}{3Ste\Delta\tau_{\text{melt}}}$$

where $\Delta\tau_{\text{melt}}$ is the nondimensional total time of melting for the particle with initial radius R_0.

References

[1] Kreith, F., Roberts, L. G., Sullivan, J. A., and Sinha, S. N., "Convection Heat Transfer and Flow Phenomena of Rotating Spheres," *International Journal of Heat and Mass Transfer*, Vol. 6, No. 10, 1963, pp. 881–895. doi:10.1016/0017-9310(63)90079-6

[2] Hsu, C., "Heat Transfer to Liquid Metals Flowing Past Spheres and Elliptical-Rod Bundles," *International Journal of Heat and Mass Transfer*, Vol. 8, No. 2, 1965, pp. 303–315. doi:10.1016/0017-9310(65)90118-3

[3] Anselmo, A., Prasad, V., Koziol, J., and Gupta, K. P., "Numerical and Experimental Study of a Solid Pellet Feed Continuous Czochralski Growth Process for Silicon Single Crystal," *Journal of Crystal Growth*, Vol. 131, Nos. 1–2, 1993, pp. 247–264. doi:10.1016/0022-0248(93)90420-2

[4] Argyropoulos, S., and Mikrovas, A., "An Experimental Investigation on Natural and Forced Convection in Liquid Metals," *International Journal of Heat and Mass Transfer*, Vol. 39, No. 3, 1996, pp. 547–561. doi:10.1016/0017-9310(95)00138-Y

[5] Argyropoulos, S., Mikrovas, A., and Doutre, D. A., "Dimensionless Correlations for Forced Convection in Liquid Metals. Part 1: Single-Phase Flow," *Metallurgical and Materials Transactions B: Process Metallurgy and Materials Processing Science*, Vol. 32, No. 2, 2001, pp. 239–246. doi:10.1007/s11663-001-0047-1

[6] Melissari, B., and Argyropoulos, S., "Measurement of Magnitude and Direction of Velocity in High-Temperature Liquid Metals. Part 1: Mathematical Modeling," *Metallurgical and Materials Transactions B: Process Metallurgy and Materials Processing Science*, Vol. 36, No. 5, 2005, pp. 691–700. doi:10.1007/s11663-005-0060-x

[7] Melissari, B., and Argyropoulos, S., "Measurement of Magnitude and Direction of Velocity in High-Temperature Liquid Metals. Part 2: Experimental Measurements," *Metallurgical and Materials Transactions B: Process Metallurgy and Materials Processing Science*, Vol. 36, No. 5, 2005, pp. 639–649. doi:10.1007/s11663-005-0054-8

[8] Melissari, B., and Argyropoulos, S., "Development of a Heat Transfer Dimensionless Correlation for Spheres Immersed in a Wide Range of Prandtl Number Fluids," *International Journal of Heat and Mass Transfer*, Vol. 48, Nos. 21–22, 2005, pp. 4333–4341. doi:10.1016/j.ijheatmasstransfer.2005.05.025

[9] Kranse, A., and Schenk, J., "Thermal Free Convection from a Solid Sphere," *Applied Scientific Research*, Vol. A15, No. 1, 1965, pp. 397–403. doi:10.1007/BF00411573

[10] Schenk, J., and Schenkels, F. M., "Thermal Free Convection from an Ice Sphere in Water," *Applied Scientific Research*, Vol. 19, No. 1, 1968, pp. 465–476. doi:10.1007/BF00383941

[11] Hao, Y. L., and Tao, Y. X., "Melting of a Solid Sphere Under Forced and Mixed Convection: Flow Characteristics," *Journal of Heat Transfer*, Vol. 123, No. 5, 2001, pp. 937–950. doi:10.1115/1.1389466

[12] Hao, Y. L., and Tao, Y. X., "Heat Transfer Characteristics of Melting Ice Spheres Under Forced and Mixed Convection," *Journal of Heat Transfer*, Vol. 124, No. 5, 2002, pp. 891–903. doi:10.1115/1.1494090

[13] Mcleod, P., Riley, D., and Sparks, R., "Melting of a Sphere in Hot Fluid," *Journal of Fluid Mechanics*, Vol. 327, 1996, pp. 393–409. doi:10.1017/S0022112096008592

[14] Nordlie, R., and Kreith, F., "Convective Heat Transfer from a Rotating Sphere," *International Developments in Heat Transfer*, ASME, New York, 1961, pp. 461–467.

[15] Sparrow, E., Eichhorn, R., and Gregg, J., "Combined Forced and Free Convection in a Boundary Layer Flow," *Physics of Fluids*, Vol. 2, No. 3, 1959, pp. 319–328. doi:10.1063/1.1705928

[16] Melissari, B., and Argyropoulos, S., "The Identification of Transition Convective Regimes in Liquid Metals Using a Computational Approach," *Progress in Computational Fluid Dynamics*, Vol. 4, No. 2, 2004, pp. 69–77. doi:10.1504/PCFD.2004.003792

[17] Voller, V. R., and Prakash, C., "A Fixed Grid Numerical Modelling Methodology for Convection-Diffusion Mushy-Region Phase Change Problems," *International Journal of Heat and Mass Transfer*, Vol. 30, No. 8, 1987, pp. 1709–1719. doi:10.1016/0017-9310(87)90317-6

[18] Lan, X. K., and Khodadadi, J. M., "Fluid Flow, Heat Transfer and Solidification in the Mold of Continuous Casters During Ladle Change," *International Journal of Heat and Mass Transfer*, Vol. 44, No. 5, 2001, pp. 953–965. doi:10.1016/S0017-9310(00)00145-9

[19] Ferziger, J. H., and Peric, M., *Computational Methods for Fluid Dynamics*, 2nd ed., Springer-Verlag, Berlin, 1999.

[20] Patankar, S. V., *Numerical Heat Transfer and Fluid Flow*, Hemisphere Publishing, Washington, D.C., 1980.

[21] Brandes, E. A., and Brook, G. B., *Smithells Metals Reference Book*, 7th ed., Butterworth Heinemann, London, 1998.
[22] Mills, K. C., *Recommended Values of Thermophysical Properties for Selected Commercial Alloys*, Woodhead Publishing Limited, Cambridge, England, 2002.
[23] Ghidersa, B., and Dusek, J., "Breaking of Axisymmetry and Onset of Unsteadiness in the Wake of a Sphere," *Journal of Fluid Mechanics*, Vol. 423, 2000, pp. 33–69.
doi:10.1017/S0022112000001701
[24] Johnson, T. A., and Patel, V. C., "Flow Past a Sphere up to a Reynolds Number of 300," *Journal of Fluid Mechanics*, Vol. 378, 1999, pp. 19–70.
doi:10.1017/S0022112098003206
[25] Nakamura, I., "Steady Wake Behind a Sphere," *Physics of Fluids*, Vol. 19, No. 1, 1976, pp. 5–8.
doi:10.1063/1.861328
[26] Schlichting, H., *Boundary Layer Theory*, 7th ed., McGraw-Hill, New York, 1979.